Impact of Metal Content on the Deactivation of a Bifunctional Hydrocracking Catalyst

July Vivas-Báez, Gerhard Pirngruber, Alberto Servia, Anne-Claire Dubreuil, David Pérez-Martínez

IMPACT OF METAL CONTENT ON THE DEACTIVATION OF A BIFUNCTIONAL HYDROCRACKING CATALYST

July C. VIVAS-BÁEZ[a], Gerhard D. PIRNGRUBER[a],* Alberto SERVIA[a], Anne-Claire DUBREUIL[a], David J. PÉREZ-MARTÍNEZ[b]

a IFP Energies nouvelles, Rond-point de l'échangeur de Solaize, France, 69360.
b Centro de innovación y tecnología ICP, ECOPETROL S.A., Km 7 vía Piedecuesta, Piedecuesta, Colombia, 681011.
Corresponding Author: Gerhard PIRNGRUBER (mailto:gerhard.pirngruber@ifpen.fr)

Keywords: deactivation, bifunctional catalyst, metal/acid balance, nitrogen poisoning, hydrocracking.

ABSTRACT

The catalytic performance of a hydrocracking bifunctional catalyst and, consequently, its activity loss depends on the balance between the metal (M) and acid (A) functions. Commonly, the metal function is reputed to stabilize catalyst activity and should, therefore, alleviate deactivation. In order to test this hypothesis, this study aimed to assess the impact of the metal oxide (MoO_3) content on the deactivation of a vacuum gasoil hydrocracking catalyst (a nickel-molybdenum sulfide dispersed on a carrier containing USY zeolite). To do so, two bifunctional catalysts with different metal oxide contents were submitted to specific operating conditions promoting catalysts deactivation, i.e., high temperature (T=418°C) and high space velocity (LHSV=3 h^{-1}). Experiments were carried out in a pilot unit with a hydrotreated VGO feedstock containing 120 ppmw of organic nitrogen. The loss in activity was measured by following the decrease of both the VGO conversion ($370°C^{+}$) and the apparent kinetic constants for the main hydrocracking reactions (cracking, hydrodenitrogenation and aromatics hydrogenation) with time on stream. The aged catalysts, sampled from three different reactor locations, were characterized by elemental, textural analysis and thermogravimetry to investigate the quantity and nature of the coke deposits. To determine

the residual activity of the hydrogenation and acid catalyst functions, catalytic tests with different model compounds (toluene and n-heptane) were carried out. It was observed that in the hydrocracking of feedstocks with high nitrogen concentration, the decrease of the metal content causes a substantial increase of the nitrogen compounds concentration in the catalytic bed. This increase significantly reduces the available acid sites and, hence, the hydrocracking activity. But at the same time, the M/A ratio is modified in favor of the metal function. The better balance of the catalyst with low metal loading results in a lower coke deposition and, consequently, a lower deactivation rate than with the catalyst with higher metal content.

1 INTRODUCTION

The hydrocracking of vacuum gasoils (VGO) is a refining process to produce mainly middle distillates (diesel and kerosene) [1–3]. This process employs bifunctional heterogeneous catalysts that combine a (de)/hydrogenation and an acid function. Commonly the (de)/hydrogenation function is provided by metal sulfides from group VIA (molybdenum, tungsten) and group VIIIA (nickel) [4–6]. Ultra-stable Y zeolites are widely used as acid components in hydrocracking catalysts [7]. In the classical bifunctional hydrocracking mechanism [8–11], the metal function serves to dehydrogenate alkanes to the corresponding alkenes. These alkenes are desorbed from the metal sites and diffuse to the acid sites, where they are protonated to carbenium ions. These carbocations undergo skeletal isomerization and cracking; their products are desorbed as alkenes which are finally hydrogenated to alkanes on metal sites. Thus, catalyst activity, stability and selectivity strongly depend on the balance between the metal and acid functions (M/A) [12–14]), the distance between these functions (Weisz's intimacy criterion) [9,11,15] and on the characteristics of the zeolite pores [15,16].

Several authors have studied the balance between the metal and acid functions (M/A). For bifunctional catalysts based on a noble metal (Pt) during the hydroisomerization and

hydrocracking reactions of n-heptane [13,14] and n-decane [17], Guisnet et al. [13,14,17,18] found that at low (M/A) ratios, the initial activity per acid site is low and increases with the increase of this ratio until reaching a stable value, which corresponds to a bifunctional mechanism limited by the acid sites. They also found that at low M/A ratio, the catalyst stability is poor because there is a fast coke formation. For high M/A values, the catalyst is well balanced (i.e., acid-catalyzed reactions become the limiting step [19]) and the reaction follows the well-known ideal bifunctional hydrocracking mechanism. Other works [20,21] also confirmed the relation between the metal loading and catalyst activity. Degnan and Kennedy [21] evaluated the hydroisomerization of n-heptane on a Pt catalyst and they found that an imbalance between the hydrogenation and the acid functions can even alter the apparent reaction network of the system. Denayer et al. [22] found a reduction in activity with an increase of the (M/A) obtained by reducing the number of acid sites. The reduction in activity is related to the decrease in acidity and consequently in cracking power.

For metal sulfide catalysts, Mendes et al. [23] quantified the amount of Brönsted acid sites available in an ammonia atmosphere during the hydroconversion of cyclohexane and found that just around 1% of the acid sites remained available in the presence of ammonia. They noted that for two well-balanced NiMo catalysts with different Mo content, there is no difference in activity or selectivity independently of the ammonia content. Pirngruber et al. [19] compared the performance of metal sulfided catalysts with different acidity levels on the hydroconversion of n-hexadecane. They found that the inhibition of the acid sites by ammonia, in association with low zeolite contents, is necessary to balance NiMo sulfide hydrocracking catalysts. They also observed a negative correlation between catalyst selectivity to isomerization reactions and zeolite loading. The impact of MoO3 loading on activity was quite small because it was mainly governed by the zeolite loading of the catalysts. In a similar work, Mendes et al. [24] confirm that ammonia helps to equilibrate the metal-acid balance in NiMo catalysts. They also evaluated catalysts with different molybdenum loadings in the n-hexadecane hydroconversion, but no noticeable evolution of the activity with Mo

loading and only a minor evolution of the maximal C16 isomer yield were observed. M.V. Bukhtiyarova et al.[25] studied the effect of sulfosalicylic acid treatment on the properties of Beta zeolite (BEA and BEA-SA) and the performance of NiW/Beta-Al_2O_3 catalysts in hexadecane hydrocracking. The total Brønsted and Lewis acid sites concentration decreased with an acid treatment and as a result, the metal-acid balance of the catalyst shifted towards enhanced metal function, providing the beneficial effect on hexadecane hydrocracking selectivity. I.G. Danilova et al.[26] worked on the impact of rare earths on the acidity of high-silica ultrastable REY zeolites and catalytic performance of NiMo/REY+Al_2O_3 catalysts in VGO hydrocracking; they found that the increase in RE_2O_3 content led to a decrease in the strong acid site density, which suppresses overcracking reactions and improves the selectivity to middle distillates.

The deactivation of bifunctional hydrocracking catalysts with VGO feeds is dominated by the poisoning involving organic nitrogen compounds and coke deposition [27–29]. N-compounds are strongly adsorbed on the catalyst surface compared with other hydrocarbon structures present in the feed [30–32]. With a longer time on stream, the adsorbed species are converted to coke [33–37]. Concerning deactivation by coke, two different mechanisms have been proposed to explain coke formation on the metal and the acid sites of bifunctional catalysts. On metal sites, it is presumed that coke results from successive dehydrogenation reactions leading to atomic carbon or partially hydrogenated intermediates that combine to form a graphitic coke [38,39]. On acid sites, it is accepted that coke results from the polymerization of dehydrogenated intermediates generated on the metal sites [40].

The deactivation of bifunctional catalysts by coking has been the subject of numerous investigations. Many of these studies were carried out on reforming catalysts, having a hydrogenation–dehydrogenation function (Pt or Pt-Re) and an acid function (Al_2O_3 or chlorinated Al_2O_3). Barbier [40] analyzed the deposited coke on a spent reforming catalyst by temperature-programmed combustion and identified the presence of two peaks, one at around 300°C and the

other at around 450°C. It was established that the low-temperature (300°C) combustion was due to the presence of coke on the metal phase. The results of Barbier determined that the amount of coke deposited on the metallic function of a bifunctional catalyst always corresponded to a small fraction of the amount of coke accumulated in the whole catalyst. Querini et al. [41] also analyzed some industrial reforming catalyst, Pt/Al_2O_3, by thermal programmed oxidation (TPO) and found that coke is deposited first on the metal and then on the acid sites. Coke on metal increases with time initially and then remains constant, while coke on the acid sites increases during the whole run. The coke deposited on the metal is more dehydrogenated than the coke deposited on the support [42]. Bartholomew [30] claimed that in the coke deactivation of reforming catalysts, coke precursors might be formed on the metal sites via hydrogenolysis.

Most studies on the effect of the metal/acid sites ratio have been carried out using platinum catalysts. In contrast, there is not much work with metal sulfide catalysts. To the best of our knowledge, they all use different model molecules, especially alkanes, to evaluate the hydroconversion reactions under conditions, not representative of the industrial process and where there is no catalyst deactivation. Therefore, this work aims to evaluate the impact of Molybdenum loading on the deactivation of a NiMo hydrocracking catalyst using a real feed. Therefore, two bifunctional catalysts with different metal oxide contents were submitted to specific operating conditions promoting catalysts deactivation in a pilot unit with a hydrotreated VGO, according to the accelerated deactivation protocol developed in our previous work [43].

2 EXPERIMENTAL SECTION

2.1 Feedstock

The feedstock was a hydrotreated blend of 71% vacuum gasoil, 16% coker gasoil and 13% light cycle oil on a weight basis. The main properties of this feed are shown in

Table 1. Dimethyl disulfide and aniline were added to the hydrotreated VGO to generate the hydrogen sulfide and ammonia partial pressures representative of the VGO mother feed. The mother feed contained a sulfur and a nitrogen content of 1.18 and 0.25 wt%, respectively.

Table 1. Feedstock properties.

Properties		Feed
Density @ 15°C	g/cm^3	0.8679
Refraction Index @ 70° C		1.4791
Sulfur	wt%	0.016
Nitrogen	ppmw	120
Aromatics content	wt%	~42
Yield of 370°C$^+$ fraction	wt%	64
Initial boiling point (IBP)	°C	131
T50 Boiling point	°C	397
Final boiling point (FBP)	°C	554

2.2 Catalysts

The reference catalyst consists of nickel-molybdenum sulfide particles dispersed on a carrier containing USY zeolite. A series of catalysts with varying metal oxide content at a constant Ni/Mo molar ratio was prepared to evaluate the impact of molybdenum content. Their molybdenum oxide contents were 25%, 50% and 75% of the molybdenum oxide content related to the reference catalyst. No modification was made to the zeolitic support. These fresh catalysts were used to determine the activity of each function at different metal oxide contents. Based on these results, the catalyst with 50% molybdenum was chosen to be subjected to the accelerated deactivation conditions developed in our previous work [43] and compare its performance with that of the reference catalyst.

The catalysts were synthesized by incipient wetness impregnation of the zeolitic support in extrudates shape with a solution containing Ni and Mo precursors. After 1.5 hours of maturation,

the solids were dried at 120°C for 12 hours and then calcined at 450 °C for 2 hours under air. No additional information on catalyst properties is given for confidentiality reasons.

2.3 Experimental set-up

The test runs were conducted in an up-flow fixed-bed pilot unit. Detailed information has been reported elsewhere [43]. The pilot plant comprised two isothermal reactors in series, loaded with the same hydrocracking catalyst diluted with inert carborundum (SiC). Thus, both reactors operate on hydrocracking reactions. The unit has a liquid sampling system between the two reactors. The gas and liquid phases from the total effluent were separated by a high-pressure separator installed downstream of the second reactor. The gaseous effluent was transferred to a gas flow meter and then analyzed online by gas chromatography, while the liquid product was sent to a stripper and finally to a storage vessel. The liquid products were characterized by density, refractive index, nitrogen and sulfur contents and simulated distillation to daily track catalyst performance.

2.4 Experimental procedure

At the beginning of the pilot unit tests, the catalyst was sulfided in situ with an atmospheric gasoil spiked with 2% wt. (%/feed) of dimethyl disulfide (DMDS) and 2% wt. aniline (%/feed) at 350°C and 14MPa. After this step, the deactivation conditions were imposed, i.e., 418°C, LHSV of 3 h^{-1}, H_2/HC = 1500 NL/L and P = 14 MPa, with the feedstock described in section 2.1. The catalyst remained at the same conditions for 30 days. The density of the liquid effluent tracked the stabilization of the catalyst. The performance was considered stable when the density variation was lower than 0.0010 g/cm^3 for 24 consecutive hours. However, in those tests, the catalyst immediately went into a deactivation regime at the conditions applied, barely showing stabilization. Therefore, in the evaluation of the experimental results, the experimental points from the first two days were not considered because the effects of the system stabilization and catalyst deactivation can be superimposed at the beginning of the test. The unit was washed with atmospheric gasoil at the end of the experiment. The catalyst was stripped and dried with hydrogen before being

unloaded. Catalyst samples taken at the end of each experiment were carefully collected to separate the particles from the inlet, middle and outlet of each catalytic bed. More information about specific experimental procedures can be found elsewhere [43].

2.5 Kinetic performance evaluation

The conversion of VGO (370°C$^+$) (Equation 1) was monitored to assess the catalytic performance. However, interpreting the raw conversion data can be misleading, especially when the conversion is high. As the conversion increases, the reactant is depleted. Consequently, the differential reaction rate decreases. A kinetic model must be established to do a rigorous analysis of reaction rates, but for the complex reaction network of the VGO, this requires a significant amount of input data [43], which was not available in our case. Therefore, for simplicity's sake, power-law models were used to calculate the apparent kinetic constants for the main reactions (cracking, hydrodenitrogenation-HDN and aromatics hydrogenation-HDA). The inhibition and deactivation were followed by the change in these constants during time on stream. The aim was to compare the different reaction rates for the two selected catalysts. A first-order [43] kinetics was assumed for both N-containing and aromatic molecules [43] (Equation 2), i.e., for HDN and HDA, respectively. To determine the apparent HDA kinetic constant, the amount of aromatic carbon was estimated through the n-d-M method according to the standard ASTM D3238.

$$\%\text{Net Conversion} = \left(\frac{\text{mass}_{\text{x feed}} - \text{mass}_{\text{x product}}}{\text{mass}_{\text{x feed}}}\right) * 100 \qquad \text{Equation 1}$$

Where x is either the 370$^+$ mass fraction, the nitrogen content or the aromatic carbon content.

$$k = \text{LHSV} * \ln(1 - \%\text{NetConversion}/100) \qquad \text{Equation 2}$$

For reactions affected by catalyst deactivation, there is a dependence of the kinetic performance on deactivation. Therefore, an exponential decay model with three parameters (Equation 3) was assumed to dissociate both phenomena for cracking reactions. In this model, the catalyst deactivation depends on the deactivation constant and time on stream (TOS) [43–45]. The alpha (α)

(1/time) parameter accounts for the activity loss rate by deactivation of the catalyst. Finally, the c parameter represents the residual activity of the spent catalysts.

$$k_{crack}=A*exp-(\alpha*TOS)+c \qquad \text{Equation 3}$$

(A+c) corresponds to the kinetic constant of the fresh catalyst at time = 0.

2.6 Samples Characterization

2.6.1 Liquid Samples Characterization

Feed and liquid products (sampled every day) were characterized by a densimeter for determining the density, by chemiluminescence for the nitrogen content, by X-Ray fluorescence spectrometry for the sulfur content and gas chromatography for the simulated distillation.

2.6.2 Catalyst Characterization

Before being characterized, the spent catalyst samples were submitted to extraction with toluene in a soxhlet extractor at 250°C for 7 h and dried under vacuum at 120°C for 12 h. Then the following analyses were carried out. The carbon, hydrogen and nitrogen contents were determined on a Thermoscientific FlashSmart equipment. Nitrogen adsorption-desorption isotherms measurements were performed in an ASAP Micromeritics apparatus to determine the catalyst surface area and total pore volume. Additionally, the catalyst was analyzed by elemental thermogravimetry on a thermobalance Mettler ToledoTGA-DSC1 coupled with a mass spectrometer. The MoS_2 sheets were visualized and analyzed by transmission electron microscopy with a JEOL JEM 2100F microscope to determine the slab length and promotion. The TEM images were recorded in the bright field mode. The average dispersion of the MoS_2 particles was calculated from the slab length distribution, assuming a hexagonal shape for the particles [46]. Finally, the promotion degree of the MoS_2 particles was investigated by TEM–EDX detection, leading to Ni/Mo ratio calculated for about 25 particles.

2.6.3 Catalytic tests with model molecules

Catalytic tests with model compounds were carried out to characterize the activity of both catalytic functions for the fresh and the spent catalysts. The hydrogenation activity was evaluated by converting toluene to hydrogenated products. For fresh catalysts, the reaction was carried out in the presence of aniline (0.5 wt %) in order to moderate their activity. In the case of spent catalysts, no aniline was used. The cracking function was determined by the hydroconversion of n-heptane to isomerization and cracking products. The used methods are analogous to the one described elsewhere [47]. The catalytic tests were carried out in a high-throughput fixed bed reactor unit in the presence of H_2S (generated by decomposition of DMDS) under hydrogen pressure. Catalysts samples were sulfided in situ. The operating conditions for each experiment are presented in Table 2.

Table 2. Operating conditions of the catalytic tests with model molecules.

		Toluene Hydrogenation		**n-Heptane Hydroconversion**
		Fresh catalyst	Spent catalyst	Fresh and spent catalysts
Concentration of reactant	wt %/feed	20*	20*	95.15
DMDS concentration	wt %/feed	6	6	4.85
Aniline concentration	wt %/feed	0.5	--	--
P	MPa	6	6	6
LHSV	h^{-1}	2	2	4
T	°C	350	350	350/360/380
H_2/HC	NL/L	450	450	330

*in cyclohexane as solvent

3 RESULTS

To evaluate the impact of the MoO_3 loading on catalyst performance, the results of the model molecule (Toluene, n-heptane) tests obtained with catalysts with different metal contents are firstly

presented. These results serve as a basis for the interpretation of the VGO hydrocracking experiments under deactivation conditions for two catalysts with different metal content, which are reported in section 3.2. Subsequently, the characterization of the spent catalysts obtained in the pilot plant tests is shown in section 3.3.

3.1 Model molecules tests for fresh catalysts with different MoO_3 contents

In Figure 1a, the hydrogenation activity of the catalysts is presented as a function of their MoO_3 content; as expected, the conversion increased with the metal oxide content. Concerning the cracking function, the lower the amount of molybdenum, the lower the activity, although all catalysts had the same zeolite content (see Figure 1b). The strong dependence of the cracking activity on molybdenum loading is quite remarkable because it is more pronounced than reported in previous studies [19,23,24]. This indicates a strong limitation of the bifunctional mechanism by the initial dehydrogenation steps.

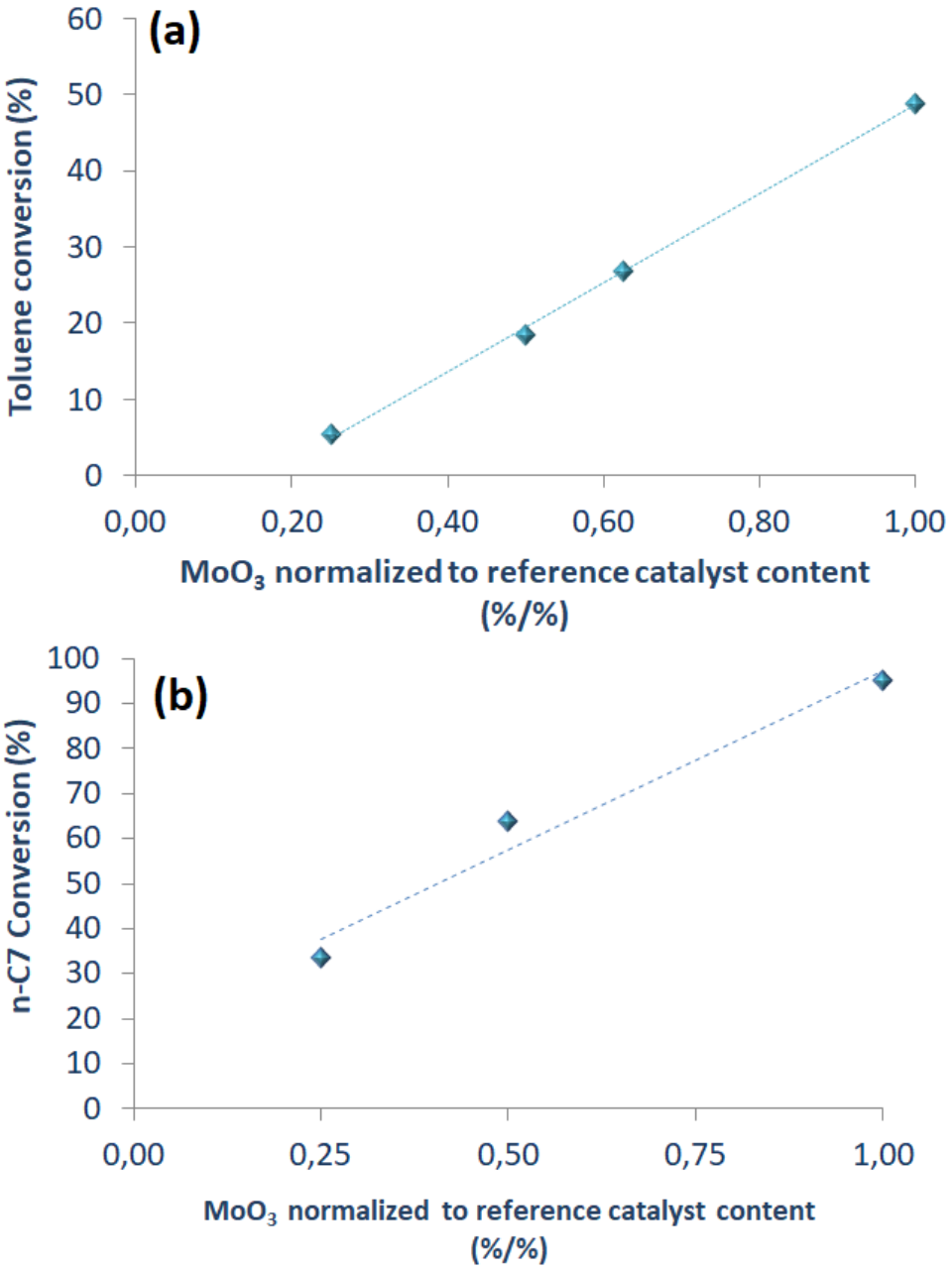

239

240 **Figure 1. Catalytic activities evaluated by model molecules catalytic tests for fresh, dried catalyst**
241 **samples with different MoO_3 contents a) Hydrogenation of toluene in the presence of aniline, b)**
242 **Isomerization/cracking of n-heptane at 360°C.**
243

244 The selectivity to i-heptane is shown in Figure 2. The results indicate that the selectivity increases
245 as the metal oxide content increases, for a given n-C_7 conversion. This is sign of a better
246 metal/acid (M/A) balance. As the metal content of the catalyst increases, the probability of an

intermediate i-C_7 olefin finding a metal site, before undergoing further isomerization and cracking increases.

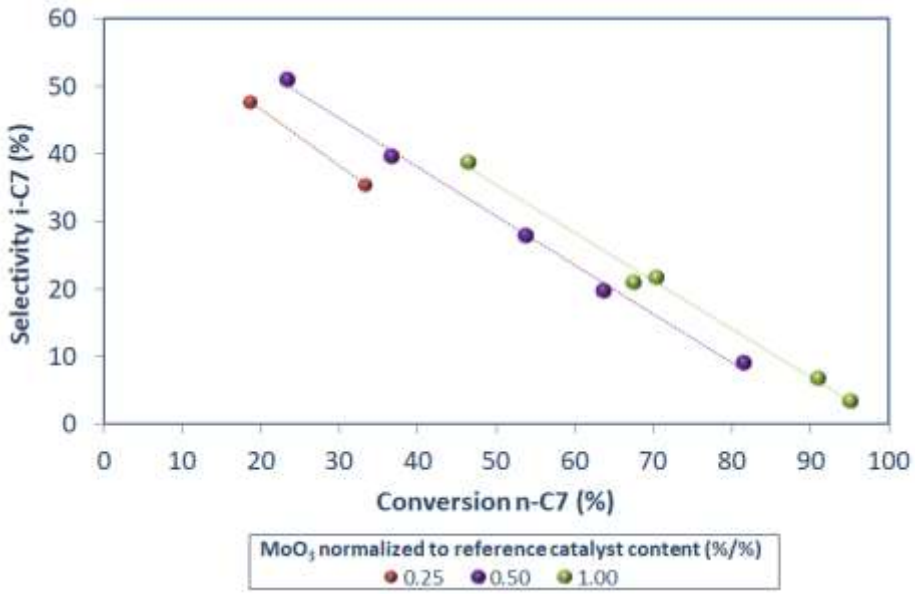

Figure 2. Selectivity to i-C_7 Vs. n-C_7 conversion for fresh dried catalyst samples with different MoO_3 contents.

Once this simple screening of the molybdenum content was accomplished, the catalyst with 50 % of the metal oxide content (designated as "0.5 MoO_3") of the reference catalyst (designated as "Reference") was selected to evaluate its loss of activity in the pilot unit under accelerated deactivation conditions. The goal was to evaluate the impact of an important modification of the M/A ratio on catalyst activity and deactivation.

3.2 Deactivation experiments with catalysts at different metal contents

3.2.1 Evolution of the apparent kinetic constants with time on stream

In the first place, the evolution of the net conversion (Equation 1) with time on stream is displayed in Figure 3 for both the first reactor and the whole system. The catalyst with the lower molybdenum content presented a lower conversion for both reactors.

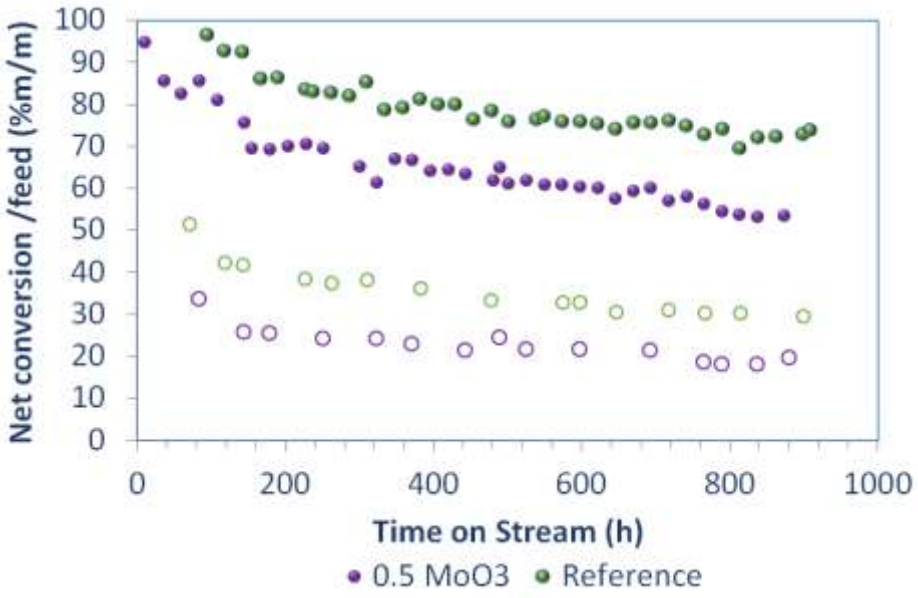

Figure 3. Net conversion as a function of time on stream for catalysts with different metal contents. Open symbols=First reactor effluent, Full symbols=Total effluent.

The evolution of the apparent kinetic constants for cracking, hydrodenitrogenation (HDN), and aromatic hydrogenation (HDA) reactions with time on stream (TOS) are shown in Figure 4, Figure 5 and Figure 6, respectively.

As was expected, the data indicate that the reduction in the amount of molybdenum (the component responsible for the hydrogenation activity) caused a decrease in the hydrogenation reactions of both aromatics and nitrogen compounds (Figure 5 and 6). Also, the cracking constants decreased by about 40%. This may be explained by two factors: (i) the limitation of bifunctional cracking by the metal function, as illustrated for n-heptane cracking in Figure 1b; (ii) the lower HDN activity, leading to a higher organic nitrogen concentration inside the reactor in the case of the 0.5MoO3 catalyst, which inhibits the cracking activity.

The kinetic rates for the mentioned reactions were lower in the first reactor than in the second one (HDA values are not shown for the first reactor since they are negligible). This result is explained by the organic nitrogen concentration profile along the system, that strongly inhibits both catalyst functions.

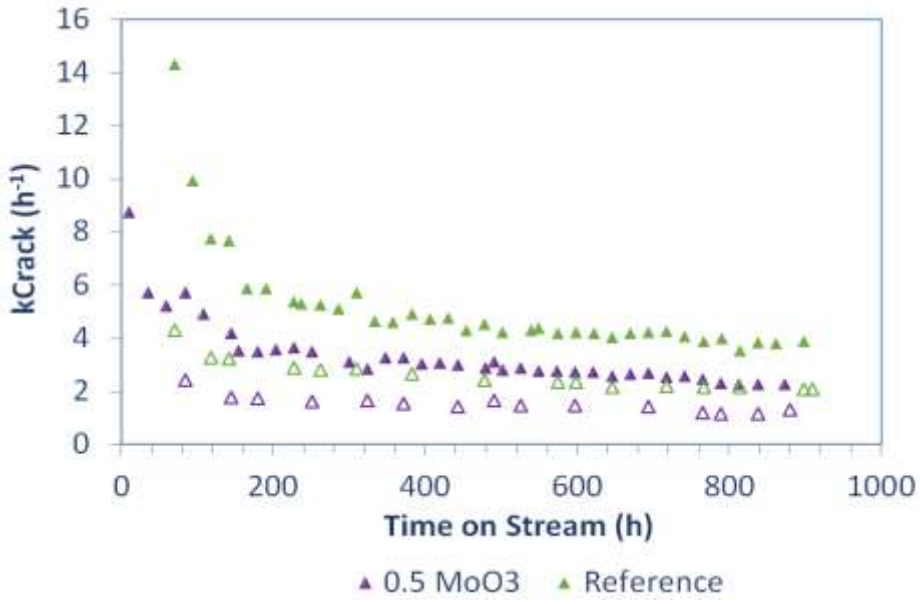

Figure 4. Global and first reactor kinetic constants as a function of time on stream for cracking reactions for catalysts with different metal contents. Open symbols=First reactor effluent, Full symbols=Total effluent.

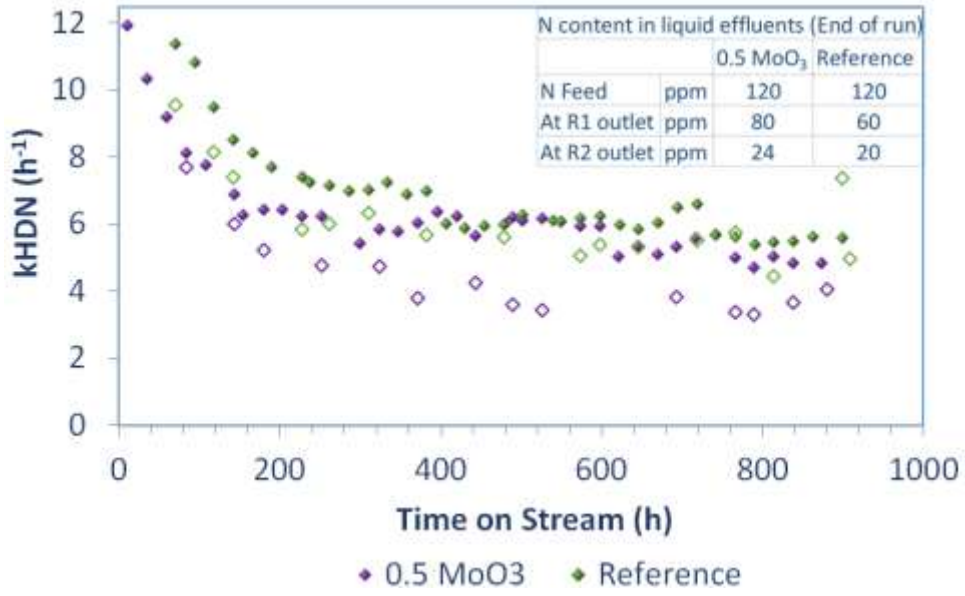

Figure 5. Global and first reactor kinetic constants as a function of time on stream for HDN reactions for catalysts with different metal contents. Open symbols=First reactor effluent, Full symbols=Total effluent.

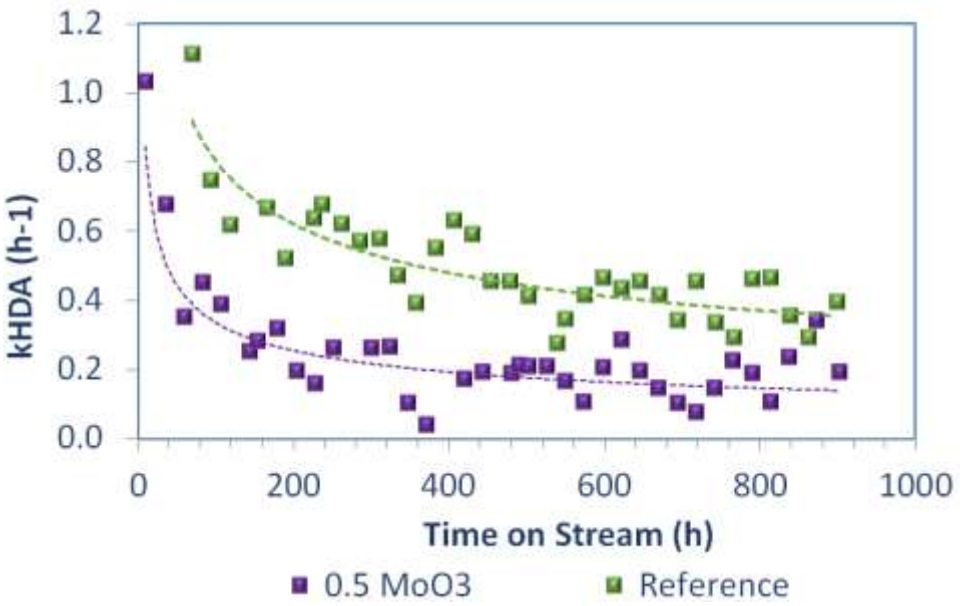

Figure 6. Global reactor kinetic constants as a function of time on stream for HDA reactions for catalysts with different metal contents.

3.2.2 Activity loss

The data of the calculated rate constants as a function of time on stream were fitted to the exponential decay model (Supporting information, Figure S1 and Figure S2) presented in section 2.5 (Equation 3). The coefficients for both catalysts are presented in

Table 3. The reference catalyst had a higher residual activity (c value) than the $0.5MoO_3$ catalyst. But the exponential decay model also indicates that the relative activity loss was faster for the catalyst with the stronger hydrogenation function and that the retained activity with respect to the initial activity was lower for this catalyst (c/(A+c)). The inspection of the raw conversion data had suggested the opposite trend, i.e., a higher conversion loss for the $0.5MoO_3$ catalyst (Figure 3). However, as previously explained, it is more accurate to examine the evolution of the reaction rate coefficients since the interpretation of the raw conversion data can be misleading because the relationship between conversion and contact time is not linear. The higher the conversion, the greater the contact time required to increase it (higher catalyst volume). So, in our case, it is not the same to lose 25 points of conversion with the reference catalyst between 97 and 72 than to lose 31 points with the catalyst of lower molybdenum content between 85 and 54 both of them

during TOS from 94h to 838h. In other words, the fact that the conversion decreases from a high conversion (97%) implies the deactivation of a larger fraction of the catalytic bed than the fraction which is deactivated for the conversion to decrease from a value of 85%. This behavior is not reflected in the conversion curve but in the kinetic constants, so the comparisons at different conversion levels should be made based on these data. For the purpose of understanding, the analysis of the evolution of apparent velocity coefficients is more appropriate."

Table 3. Activity loss rate coefficients (α) and residual activities (c) calculated with an exponential decay model for catalysts with different metal contents.

Catalyst	α	A	c	c/(A+c)
	(1/day)			
0.5 MoO_3	0.23	5.7	2.7	0.32
Reference	0.39	29	4.3	0.13

3.3 Spent catalysts characterization

3.3.1 Elemental analysis

The carbon content of the spent samples is presented in Figure 7. Contrary to what was expected, the carbon deposition was lower for the catalyst with lower metal content. This behavior can be attributed to the higher nitrogen concentration (lower k_{HDN} values) in the liquid phase with this catalyst, which inhibits cracking reactions and, consequently, the polymerization reactions to form coke. The values of the N/C ratio (Figure 8) as well as the nitrogen content in coke (Figure 9) confirmed the latter. The nitrogen content was higher for the spent catalysts with lower molybdenum loading. It means that the contribution to the overall coke formation from nitrogen precursors plays a more important role for this catalyst in comparison with the reference catalyst. For both catalysts, the carbon content along the reactor increased from the inlet to the outlet; meanwhile, the N/C values decreased. Both facts agree with the nitrogen concentration profile, which decreases along the length of the reactor. The preferential adsorption of the nitrogen

compounds on acid sites inhibits the polymerization of the dehydrogenated intermediates reducing the formation of coke deposits.

Figure 7. Carbon contents of the spent catalysts with different metal contents. Samples taken at different reactor locations.

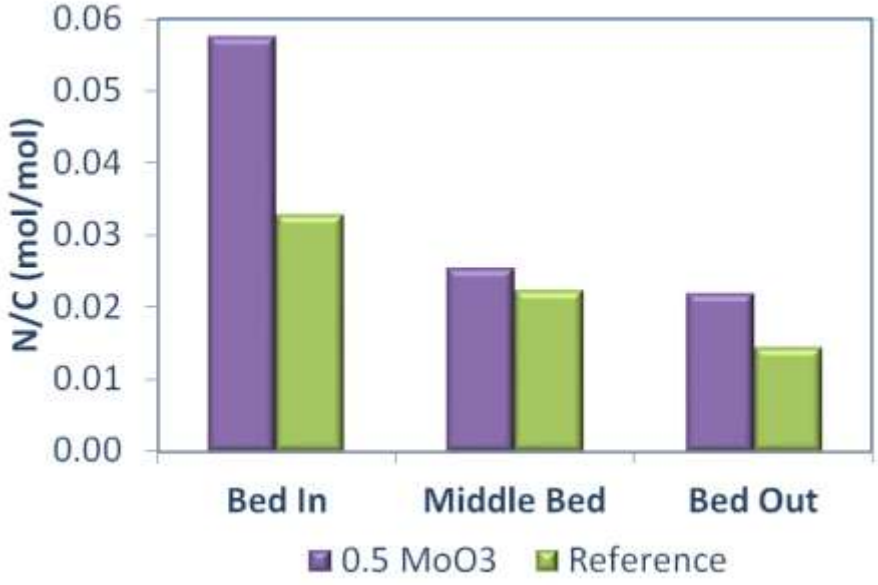

Figure 8. N/C ratio of the spent catalysts with different metal contents. Samples taken at different reactor locations.

Figure 9. Nitrogen content of the spent catalysts with different metal contents. Samples taken at different reactor locations.

Results of the H/C ratio of the coke in the spent catalysts are shown in Figure 10. A lower H/C ratio (indicating a more aromatic character of the coke deposit) was observed for the carbon deposits formed on the reference catalyst than for the $0.5MoO_3$ catalyst. It can be related to the higher cracking rate of the reference catalyst, which enhances the polymerization reactions of the coke precursors, forming more condensed structures with lower H/C ratios and with more dehydrogenation reactions. The H/C ratio (Figure 10) diminished along the catalytic bed.

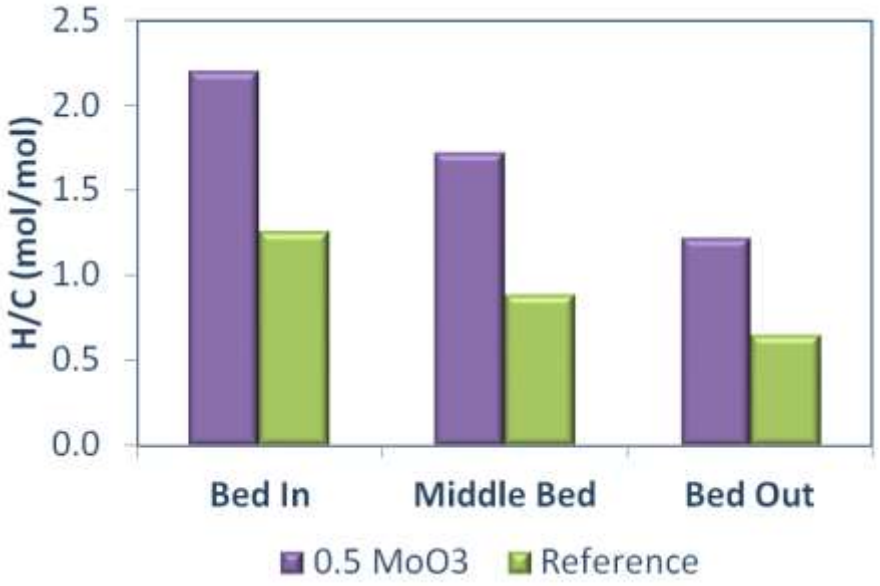

Figure 10. Hydrogen/Carbon ratio of the spent catalysts with different metal contents. Samples taken at different reactor locations.

Analysis of coke composition suggests that a proportion of the global coke originates from organic nitrogen species. However, as HDN proceeds through the reactor and nitrogen is removed, other mechanisms, such as aromatic coke formation, begin to play a more important role in catalyst deactivation. This corresponds to the results obtained in our previous work [43].

3.3.2 Textural Analysis

Catalysts were also analyzed by nitrogen adsorption-desorption isotherms. The surface area (A_{BET}) and pore volume (PV) with respect to the fresh catalyst are presented in Table 4. The area and volume losses for each catalyst show a direct correlation with its carbon deposition. Thus, the most significant modifications of the textural properties of the catalyst were found for the reference catalyst. A more pronounced decrease of surface and pore volume happened at the bed outlet, agreeing with the higher carbon content at this location. Table 4 also shows the ratio between the hysteresis area of each spent catalyst and the corresponding fresh catalyst, following the methodology suggested by Sámano et al. [48]. The higher the value, the higher the extent of catalyst

deactivation. The data showed a higher deactivation with the reference catalyst than with the one containing less molybdenum. The reactor outlet values were also higher than at the reactor inlet for the two spent catalysts, consistent with the textural and the elemental results.

Table 4. Characterization of spent catalysts with different metal contents: Surface area (A_{BET}), total pore volume (PV), micropore volume (μVol) and the ratio of hysteresis area (HA) of the spent catalyst relative to the fresh catalyst.

Catalyst	$A_{BET}/A_{BETfresh}$		PV/PV_{fresh}		$\mu Vol/\mu Vol_{fresh}$		$\frac{HA_{Spent\ Catalyst}}{HA_{Fresh\ Catalyst}}$	
	Bed Inlet (%)	Bed Outlet (%)	Bed Inlet (%)	Bed Outlet (%)	Bed Inlet (%)	Bed Outlet (%)	Bed Inlet	Bed Outlet
0.5 MoO_3	82	78	85	79	68	63	1.13	1.28
Reference	82	71	78	69	61	65	1.33	1.49

3.3.3 Thermo-gravimetric Analysis

TGA analyses were done to characterize the coke deposits on the spent catalysts. The first time-derivative of weight loss as a function of temperature is illustrated in Figure 11. The first peak, around 100°C, corresponds to H_2O desorption, the second one (280-330°C) corresponds mainly to SO_2 release and the last peak is associated with the combustion of the coke deposits [49,50]. In

Table 5, the percentage of the weight loss within the range of temperature corresponding to coke deposits combustion is presented. These values agree with the carbon content from elemental analysis (see Figure 7).

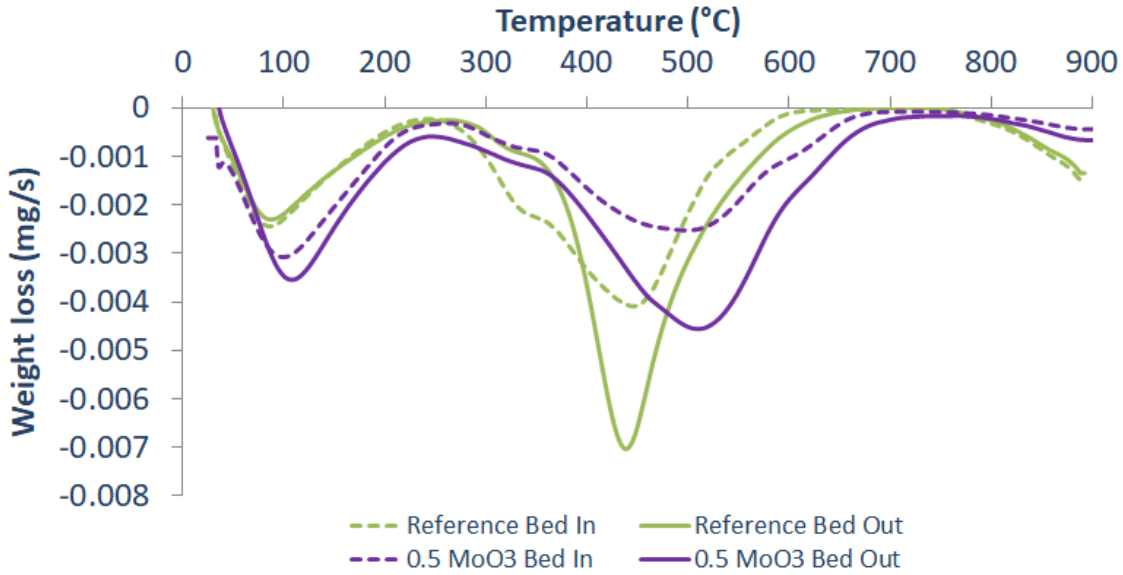

Figure 11. TGA profiles of bed inlet and bed outlet samples from the spent catalysts with different metal contents. Dotted line=First reactor effluent, continuous line=Total effluent.

The maximum weight loss temperature is an indicator of the nature of coke; the higher this temperature, the more difficult to combust the coke is. It is often associated with a lower H/C ratio of the coke deposits. However, the coke deposits on the catalyst with less metal concentration required a higher temperature to combust (Figure 11 and

399 Table 5), although its H/C ratio is higher (Figure 10). This behavior suggests that the high-
400 temperature peaks for this catalyst were related to the higher nitrogen content of its coke deposits
401 (Figure 9). This is in agreement with the work of Zeuthen et al. [35], who characterized some aged
402 hydroprocessing catalysts by temperature-programmed oxidation and identified that the strongly
403 adsorbed organic-nitrogen species are oxidized at temperatures around 500°C.

404

Table 5. Estimation of CO_2 weight loss of the coke deposits and maximum peak temperature from TGA profiles for spent catalysts with different metal contents.

Catalyst	CO_2 weight loss (wt %)	Maximum Peak Temperature (°C)
0.5 MoO_3 Bed In	7.8	495
0.5 MoO_3 Bed Out	10.3	510
Reference Bed In	11.2	445
Reference Bed Out	16.6	440

3.3.4 Model molecule tests

The residual activity of the (de)/hydrogenation and the acid functions of the spent catalysts were characterized by toluene hydrogenation and n-heptane hydroconversion, respectively. Figure 12 illustrates the first-order rate constant of the spent catalysts relative to the corresponding fresh catalyst ($k_{Hydro\ fresh}$) for both studied catalysts during toluene hydrogenation (k_{Hydro}). These values reveal that, despite its lower initial activity, the catalysts with the lower metal content retained more hydrogenation activity than the reference catalyst, which lost around 80% of its original activity. The reasons for this will be discussed in the next section. The activity loss of the metal function increased along the catalytic bed for both samples.

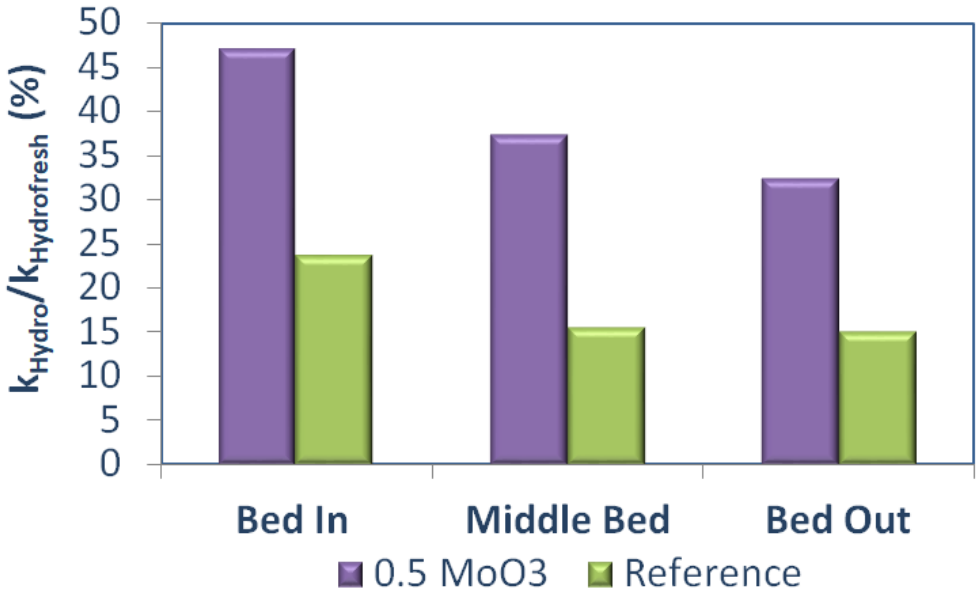

Figure 12. Residual catalytic hydrogenation activity of the spent catalysts relative to the fresh catalysts, evaluated by toluene hydrogenation. Samples taken at different reactor locations.

Regarding the n-heptane cracking activity results (Figure 13), it was noticeable that it was severely deactivated in both cases. All the residual activities were below 5%. Note that, as illustrated in Figure 1b, the n-heptane cracking activity is not an exclusive measure of the acid function, but rather presents the overall bifunctional hydrocracking activity of the catalyst. For the catalyst with lower molybdenum content, the differences along the reactor were negligible. The reference catalyst had a significantly higher residual cracking activity (in absolute and in relative terms) at the bed outlet. This is attributed to the difference in nitrogen content of the carbon deposits. The reference catalyst had a significantly lower N/C ratio at the bed outlet. It seems that the nitrogen in the coke is the main cause of the decrease in residual cracking activity. We had already pointed out in our previous work[51] that the residual acidity of the catalyst was decorrelated from the total coke content and specifically related to nitrogen compounds.

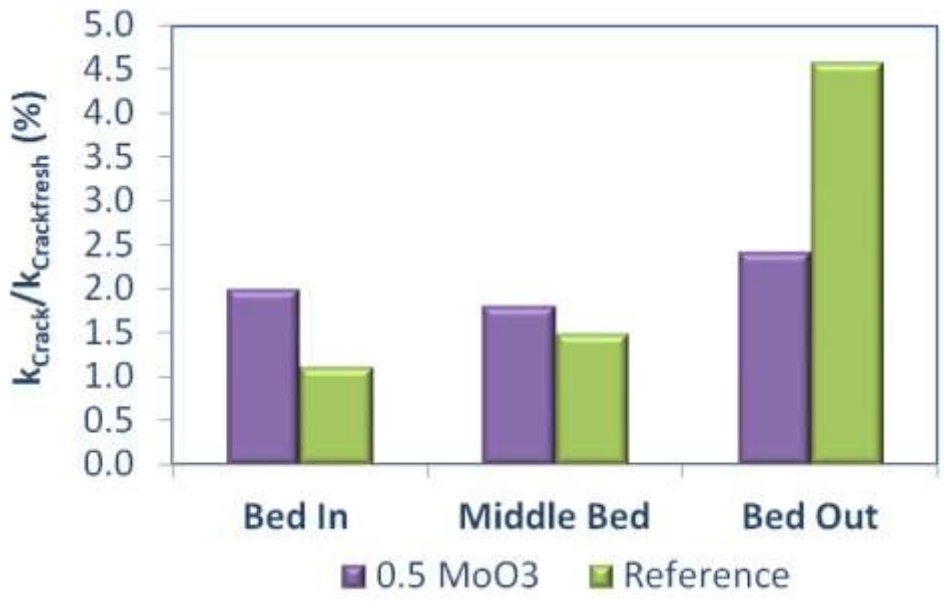

Figure 13. Residual catalytic cracking activity of the spent catalysts relative to the fresh catalyst, evaluated by isomerization/cracking of n-heptane at 360°C. Samples taken at different reactor locations.

The selectivity to i-heptane is presented in Figure 14. In contrast to the fresh samples, the 0.5 MoO_3 catalyst had a higher i-heptane selectivity, meaning that the ratio between the metal and

acid sites (M/A) was better balanced for this catalyst. This is in line with the higher residual hydrogenation activity (Figure 12) and the lower residual cracking (Figure 13) of the 0,5 MoO_3 catalyst.

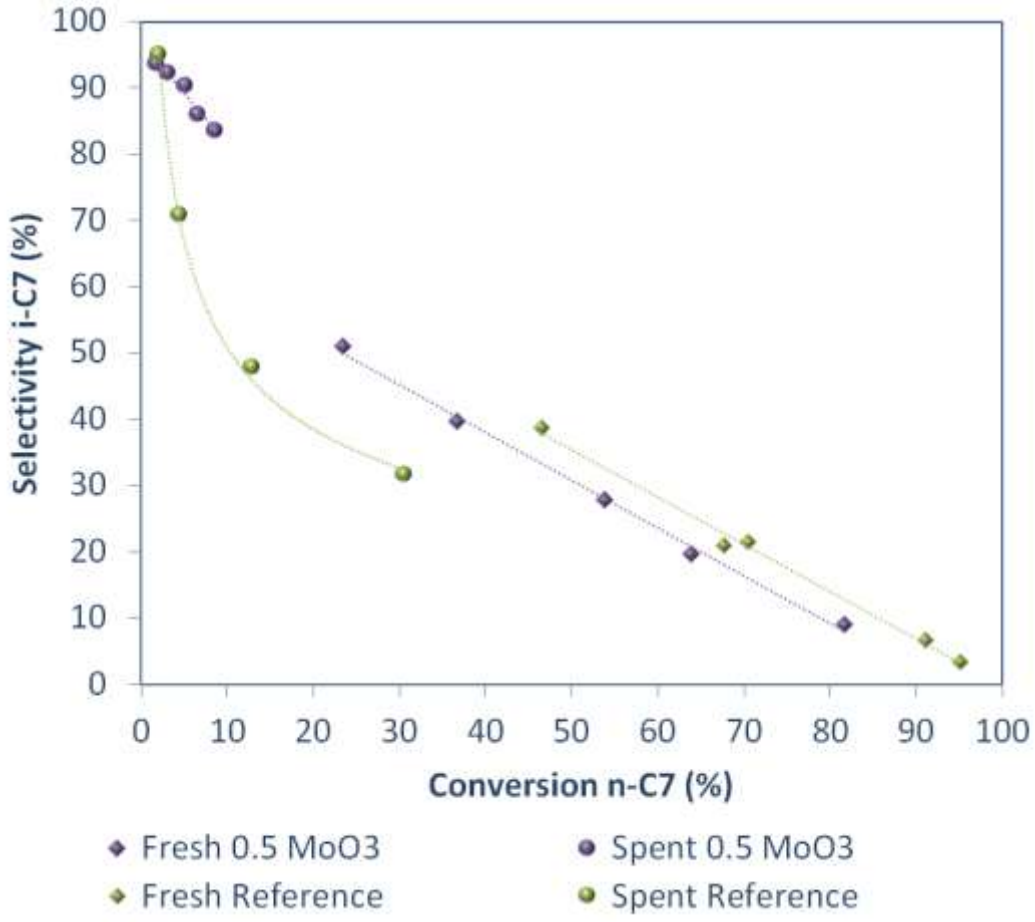

Figure 14. Selectivity to i-C_7 Vs. conversion n-C_7, obtained by n-heptane hydroconversion at different temperatures.

4 DISCUSSION

Hydrocracking proceeds by bifunctional catalysis. This makes studying the deactivation very complex, because the deactivation of the overall hydrocracking activity depends on the deactivation of the metal and of the acid function as well as on the evolution of the balance between the two. We, therefore, started by evaluating the impact of metal/acid balance on the

activity of fresh catalysts in model reactions. As expected, on fresh catalysts, the hydrogenation activity increased (almost proportionally) with the molybdenum content (Figure 1Figure 1a). The decrease in the metal content also had a negative impact on the activity of the cracking function (Figure 1b). This result agrees with other authors [14], who established that at low metal/acid (M/A) ratios, there is a limitation of the bifunctional mechanism by the (de)-hydrogenation steps. This means that the metal sites are not sufficiently abundant to provide olefins for all the acid sites, so the maximum activity of the cracking function cannot be exploited. A decrease in the overall activity of the catalyst is then observed. The fact that the decrease is more pronounced than in some other recent studies on sulfide hydrocracking catalysts [19,23,24] indicates that our catalysts covered a range of lower M/A ratios than the works cited above.

During the pilot plant deactivation experiments, the following differences in the behavior of the 0.5 MoO_3 catalyst with respect to the reference catalyst were observed in terms of reactivity:

- A lower cracking activity, but also a slower (relative) deactivation.
- A lower hydrodenitrogenation (HDN) and aromatics hydrogenation (HDA) activity.

In terms of characterization of the spent catalyst, it was observed that the 0.5 MoO_3 catalyst:

- Had a lower amount of coke, associated with a lower loss of surface area and pore volume.
- Had a higher nitrogen content (and, thus, a higher N/C ratio).
- Retained a higher percentage of its initial hydrogenation activity.
- Retained a higher percentage of its initial cracking activity at the bed inlet, but a lower percentage at the bed outlet.

In the following discussion, we will try to rationalize these trends. In our earlier work, we had seen that the deactivation process is largely governed by the presence of organic nitrogen species, which in turn determines the metal/acid balance [43]. The lower the HDN activity, the higher is the nitrogen compounds' concentration along the catalytic bed. This higher concentration has a strong repercussion on the catalytic performance since nitrogen derivatives are known to be inhibitors of

475 the metal sites [43,52–55] and especially of the acid sites [23,43], where they are strongly adsorbed [56–59].
476 The inhibition of the acid and metal sites has two antagonistic effects with respect to coke
477 formation. On the one hand, the adsorbed nitrogen compounds may eventually be converted to
478 coke, permanently deactivating the acid sites. Moreover, the inhibition of the hydrogenation activity
479 of the metal sites leads to an increase in aromatics concentration along the reactor. If there are
480 sufficiently available acid sites, the aromatics undergo addition, dehydrogenation and hydrogen
481 transfer reactions to grow into large polyaromatic molecules, i.e., coke precursors [3,60]. On the other
482 hand, this coke deposition from aromatics is slowed down by the progressive inhibition of acid
483 sites by nitrogen compounds [61]. The data shown in this paper demonstrate that the latter effect
484 dominates over the former ones. Despite its lower HDN and HDA activity, i.e., despite of a higher
485 concentration of coke precursors, the 0.5 MoO_3 catalyst generated less coke. This must be related
486 to the lower availability of acid sites (i.e., a stronger inhibition by nitrogen compounds with respect
487 to the reference catalyst).
488 The spent catalyst samples with the lower molybdenum concentration presented higher nitrogen
489 contents and higher N/C ratios than the spent reference catalyst, especially at the bed inlet (Figure
490 8 and Figure 9), meaning that the contribution of nitrogen compounds to the overall coke formation
491 was higher for this catalyst. This result is linked to the more nitrogen-rich atmosphere in the reactor
492 when the 0.5 MoO_3 catalyst was used. The reference catalyst exhibited a higher amount of coke
493 with less nitrogen, i.e., a more significant contribution to the global coke formation came from
494 aromatic compounds (whose condensation reactions are catalyzed by the acid sites). This can
495 also explain the lower H/C ratio (Figure 10) of these samples.

496 Regarding the residual activities of the spent samples, it was observed that the loss of
497 hydrogenating activity was more pronounced for the reference catalyst (Figure 12). Since no
498 meaningful differences were observed in sintering or depromotion between the spent samples
499 (Supporting information table S1, TEM analysis), this behavior was attributed to a higher coke

build-up with the reference catalyst. In reference [51], we had already observed a strong correlation between the amount of coke formation and the loss of hydrogenation activity. The coke deposition is determined by the metal/acid (M/A) balance. Figure 14 shows that the M/A balance was less favorable for the spent reference catalyst (less metal sites vs. acid sites). This explains the higher coke formation on this catalyst, which in turn leads to a strong deactivation of the metal function (this feedback loop will be discussed later in the text).

The residual n-heptane hydrocracking activity was very low for both samples. The 0.5 MoO_3 catalyst had a lower cracking activity than the reference catalysts at the bed outlet (Figure 913). This is attributed to the higher nitrogen content of the coke on the 0.5 MoO_3 samples (Figure 9 because the nitrogen species are strongly adsorbed on the acid sites, deactivating them. As mentioned before, this catalyst exhibited a lower carbon deposition, which can be attributed to a more favorable M/A balance.

When making the link between the results of the model molecule tests and the VGO deactivation experiments, we see that the 0.5 MoO_3 catalyst generated less coke and lost less VGO hydrocracking activity (in relative terms, see Figure 4 and Table 3).The latter observation is seemingly in contradiction with Figure 13, which shows that it lost, on average, a higher percentage of its residual n-heptane cracking activity. In order to resolve this dilemma, we have to make the hypothesis that the M/A balance does not have the same impact in n-heptane cracking and in the VGO deactivation test. In n-heptane cracking, the fresh reference catalyst was fairly well balanced, but became extremely badly balanced after deactivation (Figure 14). We hypothesize that this did not strongly impact its n-heptane hydrocracking activity, but had strong repercussions on its VGO hydrocracking activity. In order words, the stronger deactivation of the reference catalyst would, after all, be mainly related to the stronger deactivation of its hydrogenation function and not of its acid function. We admit, however, that this is just a hypothesis for moment, which should be confirmed by complementary experimentation.

Let us finally come back to the above-mentioned negative feedback loop of deactivation. If we have a hydrocracking catalyst with a strong hydrogenation function (our reference catalyst), it will lead to a quick drop of the organic nitrogen profile in the reactor. This leads in turn to an imbalance of the M/A ratio. This imbalance is the main cause of coke formation. Unsaturated coke precursors produced on the acid sites undergo polymerization reactions before being hydrogenated and successive dehydrogenation reactions occurred on metal sites leading to partially hydrogenated intermediates that combine to form coke. The formed coke deactivates both functions, but in a more significant way the hydrogenation function [51], since the cracking function is mainly affected by the nitrogen compounds. This phenomenon leads to a negative feedback loop, which is illustrated in Figure 15. When the hydrogenating function is deactivated by coke build up, the nitrogen concentration increases progressively. Therefore, more acid sites are neutralized so that the M/A balance tends to recover, and coke formation slows down. In other words, the coke formation provides negative feedback on deactivation; thus, the deactivation rate slows down over time.

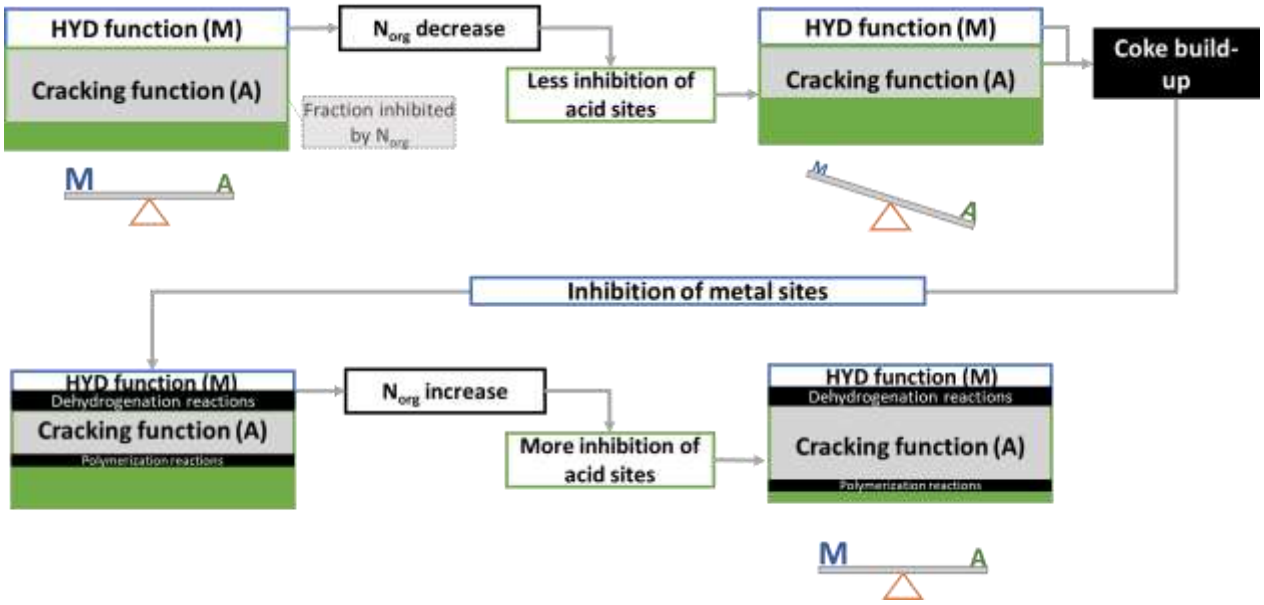

Figure 15. Schematic representation of the deactivation cycle of the acid and hydrogen functions of a bifunctional catalyst in a nitrogen-rich atmosphere. The hydrogenation function is represented by a blue rectangle, the cracking function by a green rectangle, coke on the metal function in black, the inhibited fraction of the cracking function in grey.

In general, our data show that the modification of the hydrogenation function of VGO hydrocracking catalysts has two main consequences: a reduction of the HDN activity and a reduction of the cracking activity. The balance between these two phenomena leads to unexpected behavior with respect to deactivation in organic nitrogen-poor atmospheres. Current literature states that a reduction in the hydrogenating function for samples with the same acid function, leads to more coke formation on the catalyst, which provokes rapid deactivation [13,14,17]. However, this study showed that this does not hold true for nitrogen-rich reaction systems. In this case, the decrease in the hydrogenating function causes an indirect decrease in the acid function of the catalyst, due to a stronger inhibition by nitrogen compounds. This provokes a modification on the M/A ratio, so the spent catalyst containing a lower Mo content actually shows a better balance. Consequently, less coke generation was observed, with a lower aromatic character, but with higher nitrogen content. Therefore, the deactivation was lower for the catalyst with a weaker hydrogenating function.

We have seen that many of the deactivation phenomena that we observed are dictated by the behavior of the organic nitrogen compounds. It would be desirable to carry out a similar study with nitrogen-poor feeds, where inhibition effects play a smaller role. However, in practice, this is not easily reconciled with the ambition of an accelerated deactivation protocol: the high concentration of organic nitrogen allows us to operate at high temperatures, which enhances deactivation.

5 CONCLUSIONS

- The balance between the metal and the acid functions determines the rate-limiting step of the bifunctional reaction mechanism. In case of a significant reduction in the metal content, the initial (de)/hydrogenation reactions may become the rate limiting step of the mechanism. Therefore, the global catalyst activity decreases.
- In hydrocracking of feedstocks with high nitrogen content, the decrease of the metal content of a bifunctional catalyst causes a substantial increase in the concentration of nitrogen compounds in the catalytic bed. This increase determines the performance of the catalyst by significantly reducing the available acid sites. Thus, there is a modification in the M/A ratio favoring a better balance of the spent catalyst resulting in a lower coke deposition and therefore, a lower deactivation rate.
- The interplay between HDN and cracking in VGO hydroprocessing leads to perverse effects, i.e., an improvement of the M/A balance when reducing the metal content, via the mechanism explained above. The direct effect of the reduction of the metal content and its indirect consequence, which is an increase in the acid sites inhibition by nitrogen, have an antagonistic influence on the deactivation behavior. The balance between both effects is expected to subtly depend on the properties of both the feed and the catalyst. This study provides a methodology for studying this complex system and a framework for interpreting the results, but one should be careful in generalizing the trends observed in this e, because

583 they may depend on the system under consideration. Therefore, for systems with lower
584 nitrogen contents, a specific study should be carried out.

585 • Our data also explains why deactivation slows down with time via an autoregulation
586 phenomenon. A strong metal function in the fresh catalyst leads to a fast initial coke build up
587 (by creating a M/A imbalance via the mechanism explained above). The coke builds up
588 specifically deactivates the metal function, thereby restoring the M/A balance and coke
589 formation slows down.

590

591 **Supporting Information:** Available as supporting information are the fits by the exponential decay
592 model and the TEM analyses of the catalysts.

593

6 References

(1) Toulhoat, H.; Raybaud, P., Eds. *Catalysis by transition metal sulphides*: *From molecular theory to industrial application*; IFP énergies nouvelles publications; Éd. Technip, 2013.

(2) Scherzer, J.; Gruia, A. J. *Hydrocracking science and technology*; Chemical industries, Vol. 66; Marcel Dekker, 1996.

(3) Speight, J. G. *The refinery of the future*, 1st edition; Elsevier; Gulf Professional Publishing, 2011.

(4) Ward, J. W. Hydrocracking processes and catalysts. *Fuel Processing Technology* 1993, *35* (1-2), 55–85. DOI: 10.1016/0378-3820(93)90085-I.

(5) Leprince, P. Petroleum refining. *Petroleum refining* 2001.

(6) *Advances in Catalysis*; Elsevier Science, 2016.

(7) Vogt, E. T.; Whiting, G. T.; Dutta Chowdhury, A.; Weckhuysen, B. M. Zeolites and Zeotypes for Oil and Gas Conversion. In; Advances in Catalysis; Elsevier, 2015; pp 143–314. DOI: 10.1016/bs.acat.2015.10.001.

(8) Weitkamp, J. Catalytic Hydrocracking—Mechanisms and Versatility of the Process. *ChemCatChem* 2012, *4* (3), 292–306. DOI: 10.1002/cctc.201100315.

(9) Batalha, N.; Pinard, L.; Bouchy, C.; Guillon, E.; Guisnet, M. n-Hexadecane hydroisomerization over Pt-HBEA catalysts. Quantification and effect of the intimacy between metal and protonic sites. *Journal of Catalysis* 2013, *307*, 122–131. DOI: 10.1016/j.jcat.2013.07.014.

(10) Coonradt, H. L.; Garwood, W. E. Mechanism of Hydrocracking. Reactions of Paraffins and Olefins. *Ind. Eng. Chem. Proc. Des. Dev.* 1964, *3* (1), 38–45. DOI: 10.1021/i260009a010.

(11) Weisz, P. B. Polyfunctional Heterogeneous Catalysis. In ; Advances in Catalysis; Elsevier, 1962; pp 137–190. DOI: 10.1016/S0360-0564(08)60287-4.

(12) Weitkamp, J. Isomerization of long-chain n-alkanes on a Pt/CaY zeolite catalyst. *Ind. Eng. Chem. Prod. Res. Dev.* 1982, *21* (4), 550–558. DOI: 10.1021/i300008a008.

(13) Guisnet, M.; Alvarez, F.; Giannetto, G.; Perot, G. Hydroisomerization and hydrocracking of n-heptane on Pth zeolites. Effect of the porosity and of the distribution of metallic and acid sites. *Catalysis Today* 1987, *1* (4), 415–433. DOI: 10.1016/0920-5861(87)80007-X.

(14) Giannetto, G. E.; Perot, G. R.; Guisnet, M. R. Hydroisomerization and hydrocracking of n-alkanes. 1. Ideal hydroisomerization PtHY catalysts. *Ind. Eng. Chem. Prod. Res. Dev.* 1986, *25* (3), 481–490. DOI: 10.1021/i300023a021.

(15) Francis, J.; Guillon, E.; Bats, N.; Pichon, C.; Corma, A.; Simon, L. J. Design of improved hydrocracking catalysts by increasing the proximity between acid and metallic sites. *Applied Catalysis A: General* 2011, *409-410*, 140–147. DOI: 10.1016/j.apcata.2011.09.040.

(16) Derouane, E. G.; Lemos, F.; Naccache, C.; Ribeiro, F. R. *Zeolite Microporous Solids: Synthesis, Structure, and Reactivity*; Springer Netherlands, 1992. DOI: 10.1007/978-94-011-2604-5.

(17) Alvarez, F.; Ribeiro, F. R.; Perot, G.; Thomazeau, C.; Guisnet, M. Hydroisomerization and Hydrocracking of Alkanes. *Journal of Catalysis* 1996, *162* (2), 179–189. DOI: 10.1006/jcat.1996.0275.

(18) Guisnet, M. “Ideal” bifunctional catalysis over Pt-acid zeolites. *Catalysis Today* 2013, *218-219*, 123–134. DOI: 10.1016/j.cattod.2013.04.028.

(19) Pirngruber, G. D.; Maury, S.; Daudin, A.; Alspektor, P. Y.; Bouchy, C.; Guillon, E. Balance between (De)hydrogenation and Acid Sites:Comparison between Sulfide-Based and Pt-Based Bifunctional Hydrocracking Catalysts. *Ind. Eng. Chem. Res.* 2020, *59* (28), 12686–12695. DOI: 10.1021/acs.iecr.0c01680.

(20) Regali, F.; Liotta, L. F.; Venezia, A. M.; Boutonnet, M.; Järås, S. Hydroconversion of n-hexadecane on Pt/silica-alumina catalysts: Effect of metal loading and support acidity on bifunctional and hydrogenolytic activity. *Applied Catalysis A: General* 2014, *469*, 328–339. DOI: 10.1016/j.apcata.2013.09.048.

(21) Degnan, T. F.; Kennedy, C. R. Impact of catalyst acid/metal balance in hydroisomerization of normal paraffins. *AIChE J.* 1993, *39* (4), 607–614. DOI: 10.1002/aic.690390409.

(22) Denayer, J. F.; Baron, G. V.; Vanbutsele, G.; Jacobs, P. A.; Martens, J. A. Evidence for Alkylcarbenium Ion Reaction Intermediates from Intrinsic Reaction Kinetics of C6–C9n-Alkane Hydroisomerization and Hydrocracking on Pt/H–Y and Pt/USY Zeolites. *Journal of Catalysis* 2000, *190* (2), 469–473. DOI: 10.1006/jcat.1999.2756.

(23) Mendes, P. S.; Silva, J. M.; Ribeiro, M. F.; Bouchy, C.; Daudin, A. Quantification of the available acid sites in the hydrocracking of nitrogen-containing feedstocks over USY shaped NiMo-catalysts. *Journal of Industrial and Engineering Chemistry* 2019, *71*, 167–176. DOI: 10.1016/j.jiec.2018.11.019.

(24) Mendes, P. S. F.; Silva, J. M.; Ribeiro, M. F.; Daudin, A.; Bouchy, C. Bridging the gap between academic and industrial hydrocracking:On catalyst and operating conditions' effects. *Catal. Sci. Technol.* 2020, *10* (15), 5136–5148. DOI: 10.1039/D0CY00568A.

(25) Bukhtiyarova, M. V.; Toktarev, A. V.; Kazakov, M. O.; Kodenev, E. G.; Pereyma, V. Y.; Gabrienko, A. A.; Bukhtiyarov, A. V.; Echevsky, G. V. Effect of sulfosalicylic acid treatment on the properties of Beta zeolite and performance of NiW/Beta-based catalysts in hexadecane hydrocracking. *Applied Catalysis A: General* 2020, *598*, 117573. DOI: 10.1016/j.apcata.2020.117573.

(26) Danilova, I. G.; Dik, P. P.; Sorokina, T. P.; Gabrienko, A. A.; Kazakov, M. O.; Paukshtis, E. A.; Doronin, V. P.; Klimov, O. V.; Noskov, A. S. Effect of rare earths on acidity of high-silica ultrastable REY zeolites and catalytic performance of NiMo/REY+Al2O3 catalysts in vacuum gas oil hydrocracking. *Microporous and Mesoporous Materials* 2022, *329*, 111547. DOI: 10.1016/j.micromeso.2021.111547.

(27) Furimsky, E. Deactivation of hydroprocessing catalysts. *Catalysis Today* 1999, *52* (4), 381–495. DOI: 10.1016/S0920-5861(99)00096-6.

669 (28) Gualda, G.; Toulhoat, H. Etude de la desactivation des catalyseurs d'hydrotraitement par
670 cokage. Synthèse bibliographique. *Rev. Inst. Fr. Pét.* 1988, *43* (4), 567–594. DOI:
671 10.2516/ogst:1988036.
672 (29) Furimsky, E. *Catalysts for upgrading heavy petroleum feeds*; Studies in surface science and
673 catalysis; Elsevier, 2007.
674 (30) Argyle, M.; Bartholomew, C. Heterogeneous Catalyst Deactivation and Regeneration: A
675 Review. *Catalysts* 2015, *5* (1), 145–269. DOI: 10.3390/catal5010145.
676 (31) Dong, D.; Jeong, S.; Massoth, F. E. Effect of nitrogen compounds on deactivation of
677 hydrotreating catalysts by coke. *Catalysis Today* 1997, *37* (3), 267–275. DOI: 10.1016/S0920-
678 5861(97)00022-9.
679 (32) Absi-Halabi, M.; Stanislaus, A.; Trimm, D. L. Coke formation on catalysts during the
680 hydroprocessing of heavy oils. *Applied Catalysis* 1991, *72* (2), 193–215. DOI: 10.1016/0166-
681 9834(91)85053-X.
682 (33) Park, Y. C.; Rhee, H.-K. The role of nickel in pyridine hydrodenitrogenation over NiMo/Al2O3.
683 *Korean J. Chem. Eng.* 1998, *15* (4), 411–416. DOI: 10.1007/BF02697131.
684 (34) Sau, M.; Basak, K.; Manna, U.; Santra, M.; Verma, R. P. Effects of organic nitrogen
685 compounds on hydrotreating and hydrocracking reactions. *Catalysis Today* 2005, *109* (1-4), 112–
686 119. DOI: 10.1016/j.cattod.2005.08.007.
687 (35) Zeuthen, P.; Blom, P.; Massoth, F. E. Characterization of nitrogen on aged hydroprocessing
688 catalysts by temperature-programmed oxidation. *Applied Catalysis* 1991, *78* (2), 265–276. DOI:
689 10.1016/0166-9834(91)80111-9.
690 (36) Zeuthen, P.; Blom, P.; Muegge, B.; Massoth, F. E. Temperature-programmed sulfidation and
691 oxidation of Ni-Mo/alumina catalysts and reaction with ammonia. *Applied Catalysis* 1991, *68* (1),
692 117–130. DOI: 10.1016/S0166-9834(00)84097-X.

(37) Zeuthen, P.; Cooper, B. H.; Clark, F. T.; Arters, D. Characterization and Deactivation Studies of Spent Resid Catalyst from Ebullating Bed Service. *Ind. Eng. Chem. Res.* 1995, *34* (3), 755–762. DOI: 10.1021/ie00042a007.

(38) Trimm, D. L. Catalyst design for reduced coking (review). *Applied Catalysis* 1983, *5* (3), 263–290. DOI: 10.1016/0166-9834(83)80156-0.

(39) Barbier, J.; Corro, G.; Zhang, Y.; Bournville, J. P.; Franck, J. P. Coke formation on bimetallic platinum/rhenium and platinum/iridium catalysts. *Applied Catalysis* 1985, *16* (2), 169–177. DOI: 10.1016/S0166-9834(00)84470-X.

(40) Barbier, J. Deactivation of reforming catalysts by coking - a review. *Applied Catalysis* 1986, *23* (2), 225–243. DOI: 10.1016/S0166-9834(00)81294-4.

(41) C.A. Querini, N.S. Figoli and J.M. Parera. Hydrocarbons reforming on Pt-Re-/Al,O,-Cl coked in a commercial reactor. *Applied Catalysis,* 1989, 249–262.

(42) Augustine, S. The effect of Re, S, and Cl on the deactivation of Pt/$gamma;-Al2O3 reforming catalysts. *Journal of Catalysis* 1989, *115* (1), 217–232. DOI: 10.1016/0021-9517(89)90020-1.

(43) Vivas-Báez, J. C.; Servia, A.; Pirngruber, G. D.; Dubreuil, A.-C.; Pérez-Martínez, D. J. Insights in the phenomena involved in deactivation of industrial hydrocracking catalysts through an accelerated deactivation protocol. *Fuel* 2021, *303*, 120681. DOI: 10.1016/j.fuel.2021.120681.

(44) M. Rashidzadeh, A. Ahmad, S. Sadighi. Studying of Catalyst Deactivation in a Commercial Hydrocracking Process (ISOMAX). *Journal of Petroleum Science and Technology* 2011, *1* (1), 46–54.

(45) Ancheyta, J.; Angeles, M. J.; Macías, M. J.; Marroquín, G.; Morales, R. Changes in Apparent Reaction Order and Activation Energy in the Hydrodesulfurization of Real Feedstocks. *Energy Fuels* 2002, *16* (1), 189–193. DOI: 10.1021/ef0101917.

(46) Lauritsen, J. V.; Bollinger, M. V.; Lægsgaard, E.; Jacobsen, K. W.; Nørskov, J. K.; Clausen, B. S.; Topsøe, H.; Besenbacher, F. Atomic-scale insight into structure and morphology changes

of MoS2 nanoclusters in hydrotreating catalysts. *Journal of Catalysis* 2004, *221* (2), 510–522. DOI: 10.1016/j.jcat.2003.09.015.

(47) Arancon, R.; Saab, M.; Morvan, A.; Bonduelle-Skrzypczak, A.; Taleb, A.-L.; Gay, A.-S.; Legens, C.; Ersen, O.; Searles, K.; Mougel, V.; Fedorov, A.; Copéret, C.; Raybaud, P. Combined Experimental and Theoretical Molecular Approach of the Catalytically Active Hydrotreating MoS 2 Phases Promoted by 3d Transition Metals. *J. Phys. Chem. C* 2019, *123* (40), 24659–24669. DOI: 10.1021/acs.jpcc.9b08437.

(48) Sámano, V.; Rana, M. S.; Ancheyta, J. An easy approach based on textural properties to evaluate catalyst deactivation during heavy oil hydrotreating. *Catalysis Communications* 2020, *133*, 105823. DOI: 10.1016/j.catcom.2019.105823.

(49) M.A. Callejas, M.T. Martínez, T. Blasco, E. Sastre. Coke characterisation in aged residue hydrotreating catalysts by solid-state 13C-NMR spectroscopy and temperature-programmed oxidation. *Applied Catalysis A: General* 2001 (218), 181–188.

(50) C.A. Querini , N.S. Figoli, J.M. Parera. Hydrocarbons reforming on Pt-Re-S/Al,O,-Cl coked in a commercial reactor. *Applied Catalysis* 1989 (52).

(51) Vivas-Báez, J. C.; Pirngruber, G. D.; Servia, A.; Dubreuil, A.-C.; Pérez-Martínez, D. J. Impact of Feedstock Properties on the Deactivation of a Vacuum Gas Oil Hydrocracking Catalyst. *Energy Fuels* 2021. DOI: 10.1021/acs.energyfuels.1c00965.

(52) Kraus, H.; Prins, R. The Effect of Phosphorus on Oxidic NiMo(CoMo)/γ-Al2O3Catalysts: A Solid State NMR Investigation. *Journal of Catalysis* 1997, *170* (1), 20–28. DOI: 10.1006/jcat.1997.1728.

(53) Hrabar, A.; Hein, J.; Gutiérrez, O. Y.; Lercher, J. A. Selective poisoning of the direct denitrogenation route in o-propylaniline HDN by DBT on Mo and NiMo/γ-Al2O3 sulfide catalysts. *Journal of Catalysis* 2011, *281* (2), 325–338. DOI: 10.1016/j.jcat.2011.05.017.

(54) *IEEE Global Telecommunications Conference and Exhibition. Communications for the Information Age*; IEEE, 1988.

744 (55) Ho, T. Poisoning effect of ethylcarbazole on hydrodesulfurization of 4,6-
745 diethyldibenzothiophene. *Journal of Catalysis* 2004, *222* (2), 450–460. DOI:
746 10.1016/j.jcat.2003.12.010.
747 (56) Celis-Cornejo, C. M.; Pérez-Martínez, D. J.; Orrego-Ruiz, J. A.; Baldovino-Medrano, V. G.
748 Identification of Refractory Weakly Basic Nitrogen Compounds in a Deeply Hydrotreated Vacuum
749 Gas Oil and Assessment of the Effect of Some Representative Species over the Performance of
750 a Ni–MoS 2 /Y-Zeolite–Alumina Catalyst in Phenanthrene Hydrocracking. *Energy Fuels* 2018, *32*
751 (8), 8715–8726. DOI: 10.1021/acs.energyfuels.8b02045.
752 (57) Khalil, I.; Celis-Cornejo, C. M.; Thomas, K.; Bazin, P.; Travert, A.; Pérez-Martínez, D. J.;
753 Baldovino-Medrano, V. G.; Paul, J. F.; Maugé, F. In Situ IR-ATR Study of the Interaction of
754 Nitrogen Heteroaromatic Compounds with HY Zeolites: Experimental and Theoretical
755 Approaches. *ChemCatChem* 2020, *12* (4), 1095–1108. DOI: 10.1002/cctc.201901560.
756 (58) C.H. Bartholomew. Mechanisms of catalyst deactivation. *Applied Catalysis A: General,* 2001,
757 17–60.
758 (59) Vogelaar, B. M.; Eijsbouts, S.; Bergwerff, J. A.; Heiszwolf, J. J. Hydroprocessing catalyst
759 deactivation in commercial practice. *Catalysis Today* 2010, *154* (3-4), 256–263. DOI:
760 10.1016/j.cattod.2010.03.039.
761 (60) Scherzer, J.; Gruia, A. J. *Hydrocracking science and technology*; Chemical industries, Vol.
762 66; Marcel Dekker, 1996.
763 (61) B.D. Muegge and F.E. Massoth. Basic studies of deactivation of hydrotreating catalysts with
764 anthracene. *Fuel Processing Technology* 1991 (29), 19–30.
765

766 TOC Graphic

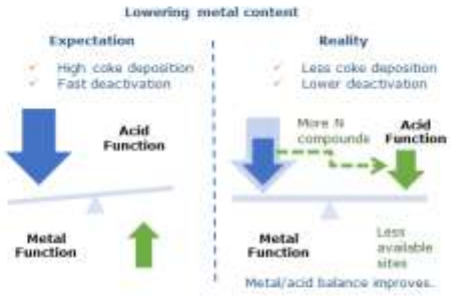

767